

# GW190814'S SECONDARY COMPONENT WITH MASS (2.50 – 2.67) M<sub>⊕</sub> AS A SUPER-FAST PULSAR

NAI-BO ZHANG<sup>1</sup> AND BAO-AN LI<sup>2\*</sup>

<sup>1</sup>Shandong Key Laboratory of Optical Astronomy and Solar-Terrestrial Environment, School of Space Science and Physics, Institute of Space Sciences, Shandong University, Weihai, Shandong, 264209, China

<sup>2</sup>Department of Physics and Astronomy, Texas A&M University-Commerce, Commerce, TX 75429, USA

\*Corresponding author: Bao-An.Li@Tamu.edu

## ABSTRACT

Using Stergioulas's RNS code for investigating fast pulsars with Equation of States (EOSs) on the causality surface (where the speed of sound equals to that of light) of the high-density EOS parameter space satisfying all known constraints from both nuclear physics and astrophysics, we show that the GW190814's secondary component of mass (2.50 – 2.67) M<sub>⊕</sub> can be a super-fast pulsar spinning faster than 971 Hz about 42% below its Kepler frequency. There is a large and physically allowed EOS parameter space below the causality surface where pulsars heavier than 2.50 M<sub>⊕</sub> are supported if they can rotate even faster with critical frequencies depending strongly on the high-density behavior of nuclear symmetry energy.

*Keywords:* Dense matter, equation of state, stars: neutron

**Introduction:** The recent LIGO/Virgo observation of GW190814 from the merger of a black hole (BH) of mass (22.2-24.3) M<sub>⊕</sub> and a secondary compact object  $m_2$  with mass (2.50 – 2.67) M<sub>⊕</sub> provided an exciting new stimulus to the ongoing debate on whether/where a gap exists between the maximum mass of neutron stars (NSs) and the minimum mass of BHs (Abbott et al. 2020). The highly unequal masses of the two objects involved and the unusually small secondary mass make the source of GW190814 unlike any other compact binary coalescence observed so far. As discussed in detail in the LIGO/Virgo discovery paper (Abbott et al. 2020), the nature of GW190814's secondary component is largely unknown as no evidence of measurable tidal effects in the signal and no electromagnetic counterpart to the gravitational waves were identified. It is thus not clear if the  $m_2$  is a BH, NS, or other exotic objects.

Already several interesting proposals have been made (see, e.g., Abbott et al. 2020; Most et al. 2020; Fishbach et al. 2020; Tan et al. 2020; Lehmann et al. 2020). Since it is well known that rotations provide additional support to the pressure balancing the gravity, leading to a NS maximum mass at the Kepler frequency about 20% higher than that of the static NS for a given nuclear Equation of State (EOS) (see, e.g., Cook et al. 1994; Lasota et al. 1996; Lattimer & Prakash 2004; Krastev et al. 2008a; Haensel et al. 2008, 2009; Breu & Rezzolla 2016; Wei et al. 2017), the possibility for the GW190814's

secondary as a rapidly rotating NS was first studied by the LIGO/Virgo Collaboration (Abbott et al. 2020). Since the spin parameter of the secondary was not observationally constrained and the calculation of the NS maximum mass depends on the unknown EOS of super-dense neutron-rich nuclear matter, conclusions regarding rotational effects on GW190814's secondary mass are not clear. In Abbott et al. (2020), taking 2.3 M<sub>⊕</sub> as the maximum mass M<sub>TOV</sub> of non-rotating NSs based on estimates from studying the merger remnant of GW170817, it was found that *although the degree of EOS uncertainty is difficult to quantify precisely if we take the more conservative 2.3M<sub>⊕</sub> bound at face value, then  $m_2$  is almost certainly not an NS*. On the contrary, Most et al. (2020) also adopted M<sub>TOV</sub> = 2.3 M<sub>⊕</sub> in a more detailed study using universal relations connecting the masses and spins of uniformly rotating neutron stars (Breu & Rezzolla 2016), it was found that *the secondary  $m_2$  does not need to be an ab-initio BH nor an exotic object; rather, it can be a rapidly rotating neutron star that collapsed to a rotating BH at some point before the merger. Moreover, a new bound of  $M_{TOV} \geq 2.08 \pm 0.04 M_{\odot}$  was obtained even in the less likely scenario in which the secondary NS never collapsed to a BH*.

While it is probably more interesting to study all other more exotic possibilities, the existing controversy calls for further studies about the GW190814's secondary simply as a rapidly rotating NS. In this work,

using Stergioulas's RNS code for investigating rapidly rotating compact stars (Stergioulas et al. 1995), we study the minimum frequency  $f_{2.5}$  that can rotationally support an NS of mass  $2.50 M_{\odot}$  (and the corresponding spin parameter  $\chi_{2.5}$ ) within the high-density EOS parameter space bounded by the NS tidal deformability from GW170817 and radii of canonical NSs from X-ray observations using Chandra-Newton and NICER as well as nuclear theories and experiments. On the causality surface where the EOSs are the stiffest physically possible, the minimum value of  $f_{2.5}$  is 971 Hz while the ratio of  $f_{2.5}$  over Kepler frequency  $f_K$ , i.e.,  $f_{2.5}/f_K$ , is between 0.578 and 0.876 (the corresponding  $\chi_{2.5}$  between 0.375 and 0.550) depending on the high-density behavior of nuclear symmetry energy. Below the causality surface, there is a large and physically allowed EOS parameter space where the secondary of GW190814 can sustain masses above  $2.50 M_{\odot}$  if they rotate even faster than those on the causality surface. Thus, within the existing bounds on the EOS from both astrophysics and nuclear physics, the GW190814's secondary component can be a super-fast pulsar spinning faster than the currently known fastest pulsar PSR J1748-2446ad of frequency 716 Hz (Hessels et al. 2006), supporting the findings of Most et al. (2020).

**An explicitly isospin dependent EOS-generator for neutron stars at  $\beta$  equilibrium:** Here we summarize the main features of an EOS-generator for NSs consisting of neutrons, protons, electrons, and muons (the  $npe\mu$  model). More details of our approach and its applications can be found in refs. (Zhang et al. 2018; Zhang & Li 2019a,b,c, 2020; Xie & Li 2019, 2020). Unlike the widely used spectral EoS and other similar piecewise parameterizations that directly parameterize the pressure as a function of energy or baryon density, we start from parameterizing the energy per nucleon in symmetric nuclear matter (SNM)  $E_0(\rho)$  and nuclear symmetry energy  $E_{\text{sym}}(\rho)$  according to

$$E_0(\rho) = E_0(\rho_0) + \frac{K_0}{2} \left( \frac{\rho - \rho_0}{3\rho_0} \right)^2 + \frac{J_0}{6} \left( \frac{\rho - \rho_0}{3\rho_0} \right)^3, \quad (1)$$

$$E_{\text{sym}}(\rho) = E_{\text{sym}}(\rho_0) + L \left( \frac{\rho - \rho_0}{3\rho_0} \right) + \frac{K_{\text{sym}}}{2} \left( \frac{\rho - \rho_0}{3\rho_0} \right)^2 + \frac{J_{\text{sym}}}{6} \left( \frac{\rho - \rho_0}{3\rho_0} \right)^3 \quad (2)$$

where  $E_0(\rho_0) = -15.9 \pm 0.4$  MeV (Brown & Schwenk 2014) is the binding energy and  $K_0 \approx 240 \pm 20$  MeV (Shlomo et al. 2006; Piekarewicz 2010; Garg & Colò 2018) is the incompressibility at the saturation density  $\rho_0$  of SNM, while  $E_{\text{sym}}(\rho_0) = 31.7 \pm 3.2$  MeV is the magnitude and  $L \approx 58.7 \pm 28.1$  MeV is the slope of symmetry energy at  $\rho_0$  (Li & Han 2013; Oertel et al. 2017), respectively. The  $K_{\text{sym}}$ ,  $J_{\text{sym}}$ , and  $J_0$  are parameters

characterizing the EOS of super-dense neutron-rich nuclear matter. They are parameters to be inferred from astrophysical observables and/or terrestrial experiments either using the direct inversion technique (Zhang et al. 2018; Zhang & Li 2019a,b,c) or the Bayesian statistical approach (Xie & Li 2019, 2020). The  $E_0(\rho)$  and  $E_{\text{sym}}(\rho)$  are then used to first construct the average nucleon energy  $E(\rho, \delta)$  in nuclear matter at nucleon density  $\rho = \rho_n + \rho_p$  and isospin asymmetry  $\delta \equiv (\rho_n - \rho_p)/\rho$  according to the isospin-parabolic approximation for the EOS of neutron-rich nuclear matter (Bombaci & Lombardo 1991)

$$E(\rho, \delta) = E_0(\rho) + E_{\text{sym}}(\rho) \cdot \delta^2 + \mathcal{O}(\delta^4). \quad (3)$$

The pressure in the  $npe\mu$  matter core of NSs is then calculated from

$$P(\rho, \delta) = \rho^2 \frac{d\epsilon(\rho, \delta)/\rho}{d\rho}, \quad (4)$$

where  $\epsilon(\rho, \delta) = \epsilon_n(\rho, \delta) + \epsilon_l(\rho, \delta)$  denotes the energy density. The  $\epsilon_n(\rho, \delta)$  and  $\epsilon_l(\rho, \delta)$  are the energy densities of nucleons and leptons, respectively. The core EOS is connected to the NV EOS (Negele & Vautherin 1973) for the inner crust and the BPS EoS (Baym et al. 1971) for the outer crust. The crust-core transition density and pressure are determined consistently from the same parametric EOS for the core. In particular, the density dependence of nuclear symmetry energy plays a very important role in determining the crust-core transition (see, e.g., Li et al. 2019, for a recent review).

As discussed in detail in Zhang et al. (2018); Zhang & Li (2019a); Xie & Li (2020), the parameterizations of both the SNM EOS  $E_0(\rho)$  and nuclear symmetry energy  $E_{\text{sym}}(\rho)$  were chosen purposely as if they are Taylor expansions of some known energy density functions, while they are really just parameterizations and the parameters are not derivatives of some known functions but to be inferred from data. Since the parameterizations become Taylor expansions of some functions asymptotically as the density approaches  $\rho_0$ , this choice allows us to use nuclear theory predictions and terrestrial nuclear experiments for the EOS parameters around  $\rho_0$  as guidances in setting the prior ranges and probability distribution functions (PDFs) in inferring their posterior PDFs from observables. Compared to directly parameterizing the normally composition-blind pressure in NSs as a function of energy or baryon density, the EOS-generator described above has the advantage of tracking explicitly the composition of the  $npe\mu$  matter in NSs. For instance, with the information about the symmetry energy, one can find easily the density profile of isospin asymmetry  $\delta(\rho)$  (or the corresponding proton fraction  $x_p(\rho)$ ) at density  $\rho$  through the  $\beta$  equilibrium condition  $\mu_n - \mu_p = \mu_e = \mu_{\mu}$  and the charge neutrality

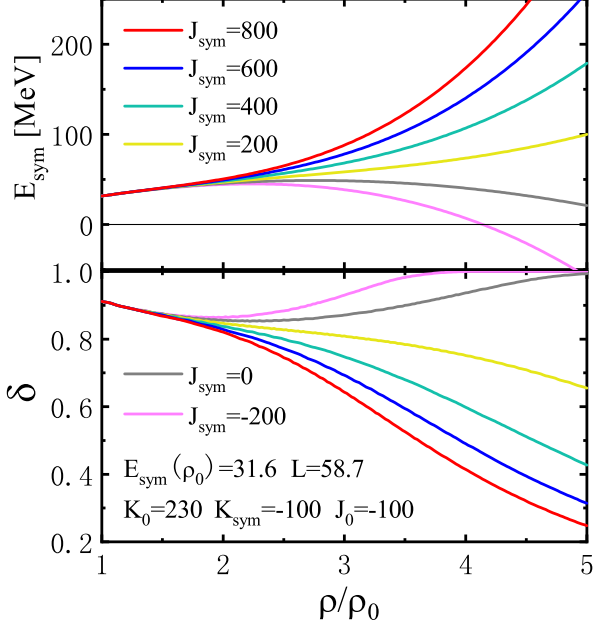


**Figure 1.** The high-density behavior of nuclear symmetry energy  $E_{\text{sym}}(\rho)$  (upper window) and the corresponding isospin asymmetry profile  $\delta(\rho)$  in NSs at  $\beta$  equilibrium (lower window) as functions of the reduced baryon density  $\rho/\rho_0$  by varying the  $J_{\text{sym}}$  parameter within its broad range predicted by nuclear theories while all other EOS parameters are fixed at the values indicated. Taken from [Zhang et al. \(2018\)](#).

condition  $\rho_p = \rho_e + \rho_\mu$  for the proton density  $\rho_p$ , electron density  $\rho_e$ , and muon density  $\rho_\mu$ , respectively. While the chemical potential of particle  $i$  can be calculated from  $\mu_i = \frac{\partial \epsilon(\rho, \delta)}{\partial \rho_i}$ .

As an example, shown in Figure 1 are the high-density symmetry energy  $E_{\text{sym}}(\rho)$  (upper window) and the corresponding isospin asymmetry profile  $\delta(\rho)$  in NSs at  $\beta$  equilibrium (lower window) as functions of the reduced baryon density  $\rho/\rho_0$  by varying the  $J_{\text{sym}}$  parameter within its broad range predicted by nuclear theories while all other EOS parameters are fixed. It is seen that the effects of varying the  $J_{\text{sym}}$  only become important above about twice the saturation density. As the  $J_{\text{sym}}$  changes from  $-200$  MeV to  $+800$  MeV, the symmetry energy changes from being super-soft to super-stiff. The corresponding isospin profile  $\delta(\rho)$  goes from very neutron-rich or  $\delta = 1$  (pure neutron matter) with the super-soft  $E_{\text{sym}}(\rho)$  to almost zero with the super-stiff  $E_{\text{sym}}(\rho)$  at super-high densities. This is well understood as the isospin fractionation due to the  $E_{\text{sym}}(\rho) \cdot \delta^2$  term in the average nucleon energy of Eq. (3). For ease of our following discussions, it is useful to emphasize that the symmetry energy term may contribute significantly to the total pressure. It is known that the total pressure around  $2\rho_0$  has strong or even dominating contributions from the symmetry energy ([Lattimer & Prakash 2000](#); [Li & Steiner 2006](#); [Li et al. 2008](#)), making the radii of canonical NSs depend strongly on the  $E_{\text{sym}}(\rho)$  around

$2\rho_0$ . At even higher densities, when the  $E_{\text{sym}}(\rho)$  is super-soft, the  $\delta$  is close to 1 as shown in Figure 1, making the  $J_{\text{sym}}$  term contribution to the total pressure as strong as the  $J_0$  term in the SNM EOS  $E_0(\rho)$  ([Xie & Li 2019](#)). Consequently, the mass-radius curve and the maximum mass of NSs are very sensitive to the high-density behavior of nuclear symmetry energy ([Li et al. 2019](#)). This also explains the findings that the radii and/or tidal deformability of canonical NSs only constrain the  $L$  and  $K_{\text{sym}}$  parameters characterizing the  $E_{\text{sym}}(\rho)$  around  $(1 - 2)\rho_0$  but not the  $J_{\text{sym}}$  parameter ([Zhang et al. 2018](#); [Xie & Li 2019](#)). To constrain the latter, one has to study the mass-radius correlations of NSs as massive as possible ([Xie & Li 2020](#)). Moreover, even for rapidly rotating NSs, it has been shown earlier using the RNS code that the mass-radius sequence, the moment of inertia, and ellipticity all strongly depend on the high-density behavior of nuclear symmetry energy ([Krastev et al. 2008a](#); [Worley et al. 2008](#); [Krastev et al. 2008b](#)). It is thus more useful to construct the EOS of NS matter by explicitly considering the isospin asymmetry at the nucleon energy level instead of directly parameterizing the pressure as a function of energy/baryon density.

The explicitly isospin-dependent NS EOS-generator described above has been used successfully in solving the NS inverse-structure problems in both the direct inversions of NS observables in the three-dimensional (3D) high-density EOS parameter space ([Zhang et al. 2018](#); [Zhang & Li 2019a,b,c, 2020](#)) or Bayesian statistical inferences of multiple EOS parameters from observational data ([Xie & Li 2019, 2020](#)). It is very efficient in generating multi-million EOSs in the allowed EOS parameter space as inputs for solving the Tolman-Oppenheimer-Volkov (TOV) NS structure equations ([Tolman 1934](#); [Oppenheimer & Volkoff 1939](#)) in the inversion processes.

The EOS-generator described above also has its limitations and drawbacks. Assuming the cores of NSs are made of only  $npe\mu$  matter even in the possibly most massive NSs, it lacks the physics associated with the possible phase transitions to exotic states of matter and/or productions of new particles, such as hyperons, mesons, and  $\Delta(1232)$  resonances, proposed in the literature. The appearance of new phases and particles is known to generally soften the EOS. Nevertheless, the EOS of  $npe\mu$  matter serves as a useful baseline for future studies incorporating the possible new phases and particles. The necessary rotational frequency calculated within the  $npe\mu$  model can be generally considered as the minimum value as a softer EOS will require a higher frequency to support a given pulsar.

**The constrained high-density EOS parameter space for massive neutron stars:** Here we illustrate

the high-density EOS parameter space  $K_{\text{sym}}-J_{\text{sym}}-J_0$  constrained by existing astrophysical observables and the causality condition. Much efforts have been devoted in recent years to constraining the high-density EOS parameters  $K_{\text{sym}}$ ,  $J_{\text{sym}}$ , and  $J_0$  using both terrestrial experiments and astrophysical observations (see, e.g., Li et al. 2014, for a comprehensive review). Unfortunately, they are still not well determined. As we shall illustrate, the high-density SNM EOS parameter  $J_0$  has the strongest control over the maximum mass of NSs. While the high-density symmetry energy parameters  $K_{\text{sym}}$  and  $J_{\text{sym}}$  mostly control the radii, tidal deformabilities, and proton fractions of massive NSs, they also have some significant influences on the maximum mass of NSs. On the other hand, while the  $L$  and  $K_{\text{sym}}$  both play significant roles in determining the radii of especially canonical NSs, they have little effects on the maximum mass of NSs. These features have been well demonstrated by many calculations using various nuclear theories and used in extracting them from astrophysical observations. However, due to the limited data available, large uncertainties still exist especially for the three high-density EOS parameters  $K_{\text{sym}}$ ,  $J_{\text{sym}}$ , and  $J_0$ . For instance, using the combined data of NS tidal deformability from GW170817 and the simultaneous measurement of mass and radius of PSR J0030+0451 by the NICER Collaboration, a very recent Bayesian analysis inferred the most probable value of  $K_{\text{sym}}$  as  $-120^{+80}_{-100}$  MeV at 68% confidence level (Xie & Li 2020). Obviously, its uncertainty is still very large. Since the available data from canonical NSs with masses around  $1.4 M_{\odot}$  reflect mostly the EOS around  $2\rho_0$  while the  $J_{\text{sym}}$  characterizes the symmetry energy at higher densities, they do not provide much constrain on the  $J_{\text{sym}}$  (Xie & Li 2019, 2020). As a result, the symmetry energy at twice the saturation is only loosely constrained to  $E_{\text{sym}}(2\rho_0) = 54.8^{+8.4}_{-19}$  MeV at 68% confidence level, while its behavior at higher densities is currently completely unconstrained as shown in Figure 1. This is well understood as we explained earlier. In the following studies, we will just use the full range of  $-200 \leq J_{\text{sym}} \leq 800$  MeV predicted by many kinds of nuclear many-body theories (see, e.g., Tews et al. 2017; Zhang et al. 2017) for surveys of model predictions for  $J_{\text{sym}}$ .

Shown in Figure 2 are the tightest constraints on the 3D high-density EOS parameter space from inverting the indicated radii and tidal deformability of canonical NSs (Zhang & Li 2020) as well as the causality condition and NSs' *minimum* maximum mass of  $M=2.14 M_{\odot}$ . The latter is the mass of PSR J0740+6620 (Cromartie et al. 2019). It is the confirmed most massive NS observed so far. So all acceptable EOSs have to be stiff enough to predict a mass-radius curve with a maximum at least as

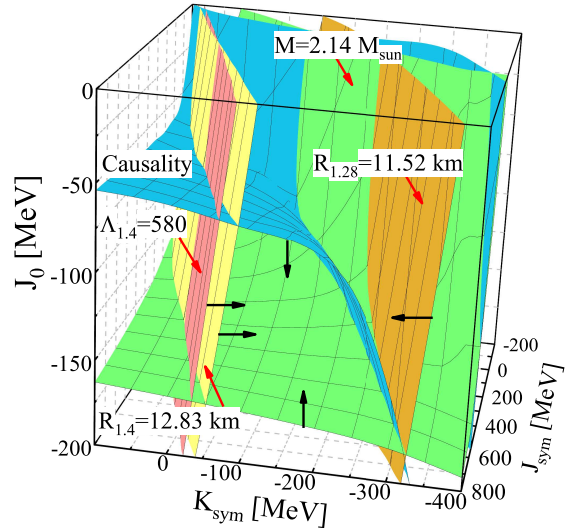


**Figure 2.** The constraints of  $M = 2.14 M_{\odot}$  (green surface),  $R_{1.4} = 12.83$  km (yellow surface),  $\Lambda_{1.4} = 580$  (red surface),  $R_{1.28} = 11.52$  km (orange surface), and causality condition (blue surface) in the 3D parameter space of  $K_{\text{sym}}-J_{\text{sym}}-J_0$ . The black arrows show the directions supporting the corresponding constraints and the red arrows direct to the corresponding surfaces. Modified from Figure 4 of Zhang & Li (2020).

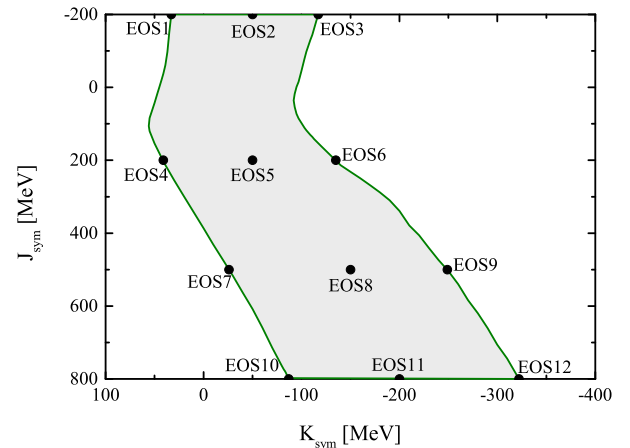


**Figure 3.** Projection of the constrained causality surface on the  $K_{\text{sym}}-J_{\text{sym}}$  plane determined by the crosslines of the constant surfaces shown in Figure 2. The shadowed range corresponds to the parameters allowed. The black dots indicate the EOS parameter sets chosen to calculate properties of pulsars on the causality surface.

high as  $2.14 M_{\odot}$ . Considering all possibly more massive NSs in the universe,  $2.14 M_{\odot}$  is the minimum maximum mass of acceptable EOSs. The surface labeled as  $M=2.14 M_{\odot}$  in Figure 2 collects all EOSs that predict a NS maximum mass of  $2.14 M_{\odot}$ . It limits the EOS space from below, while the upper bound is from the causality surface (blue) on which the speed of sound equals the speed of light ( $v_s^2 = dP/d\epsilon = c^2$ ) at the central density of

the most massive NS supported by the nuclear pressure at each point with the specific EOS there (Zhang & Li 2019a). Both surfaces are strongly controlled by the SNM EOS parameter  $J_0$ . As expected, these two surfaces are also significantly influenced by the high-density

symmetry energy especially when the  $E_{\text{sym}}(\rho)$  becomes super-soft with negative values of  $K_{\text{sym}}$  and/or  $J_{\text{sym}}$ . For example, with the super-soft  $E_{\text{sym}}(\rho)$ , to support the same NS maximum mass of  $M=2.14 M_{\odot}$ , the necessary value of  $J_0$  has to become higher as one expects.

**Table 1.** The labels and parameter sets of 12 EOSs on the bounded causality surface shown in Figure 2 and Figure 3, the resulting maximum mass  $M_{\text{TOV}}$  of non-rotating NSs, the maximum mass  $M_{\text{RNS}}$  of NSs rotating at the Kepler frequency  $f_K$ , the equatorial radius  $R_{\text{RNS}}$  of the NS with  $M_{\text{RNS}}$ , the equatorial radius  $R_{2.5}$  of the NS with mass  $2.50 M_{\odot}$  rotating at  $f_{2.5}$ , the minimum frequency  $f_{2.5}$  that can rotationally support an NS with mass  $2.50 M_{\odot}$ , the ratio  $f_{2.5}/f_K$ , and the minimum spin parameter  $\chi_{2.5}$  necessary to rotationally support the NS with mass  $2.50 M_{\odot}$ .

	$(K_{\text{sym}}, J_{\text{sym}}, J_0)$ (MeV)	$M_{\text{TOV}}$ ( $M_{\odot}$ )	$M_{\text{RNS}}$ ( $M_{\odot}$ )	$R_{\text{RNS}}$ (km)	$R_{2.5}$ (km)	$f_{2.5}$ (Hz)	$f_{2.5}/f_K$	$\chi_{2.5}$
EOS1	(33, -200, 112.5)	2.39	2.87	14.77	11.92	971	0.578	0.375
EOS2	(-50, -200, 193.2)	2.29	2.73	14.47	12.83	1318	0.781	0.550
EOS3	(-117, -200, 225.2)	2.14	2.53	13.56	—	—	—	—
EOS4	(41, 200, -69.6)	2.30	2.77	15.04	12.86	1217	0.757	0.516
EOS5	(-50, 200, -75.6)	2.28	2.73	14.47	12.80	1318	0.876	0.549
EOS6	(-135, 200, -199.4)	2.14	2.55	13.67	—	—	—	—
EOS7	(-26, 500, -68.1)	2.33	2.80	15.30	12.67	1145	0.726	0.473
EOS8	(-150, 500, -88.0)	2.30	2.76	14.67	12.46	1265	0.759	0.514
EOS9	(-249, 500, -158.6)	2.14	2.59	13.93	—	—	—	—
EOS10	(-87, 800, -65.2)	2.34	2.83	15.42	12.61	1073	0.683	0.444
EOS11	(-200, 800, -77.7)	2.34	2.83	14.95	12.36	1117	0.681	0.451
EOS12	(-322, 800, -184.1)	2.14	2.62	14.49	—	—	—	—

NOTE—Though the maximum mass of neutron stars rotating at Kepler frequency for EOS3, EOS6, EOS9, and EOS11 is larger than  $2.50 M_{\odot}$ , their maximum mass is too close to  $2.50 M_{\odot}$  for the RNS to output the  $f_{2.5}$  sequences.

We considered several reported radius and tidal deformability measurements, such as  $10.62 < R_{1.4} < 12.83$  km from analyzing quiescent low-mass X-ray binaries (Lattimer & Steiner 2014), the dimensionless tidal deformability  $70 \leq \Lambda_{1.4} \leq 580$  from the refined analysis of GW170817 data (Abbott et al. 2018), the mass and radius of PSR J0030+0451  $M = 1.44^{+0.15}_{-0.14} M_{\odot}$  and  $R = 13.02^{+1.24}_{-1.06}$  km (Miller et al. 2019) or  $M = 1.34^{+0.16}_{-0.15} M_{\odot}$  and  $R = 12.71^{+1.19}_{-1.14}$  km (Riley et al. 2019) from NICER. Both the upper and lower limits of radii from these measurements are consistent. The ones shown in the Figure 2 provides the strongest constraint on the  $K_{\text{sym}} - J_{\text{sym}}$  correlation. We notice that the lower boundary from  $R_{1.28} = 11.52$  km is just outside the crossline between the causality surface and constant maximum mass surface of  $M=2.14 M_{\odot}$ . It is known that the extraction of the lower limit of  $\Lambda_{1.4}$  from GW170817

suffers from large uncertainties and is largely model dependent. The constant surface of  $\Lambda_{1.4}=70$  is actually on the left of the  $R_{1.28} = 11.52$  km surface, thus not shown here. The almost vertical surfaces of the radius and tidal deformability indicate that they are not much affected by the high density SNM EOS parameter  $J_0$ .

The constraints of  $M = 2.14 M_{\odot}$  (green surface),  $R_{1.4} = 12.83$  km (yellow surface), and causality condition (blue surface) together enclose the allowed high-density EOS parameter space in  $K_{\text{sym}} - J_{\text{sym}} - J_0$ . In particular, the causality surface determines the absolutely maximum mass  $M_{\text{TOV}}$  of non-rotating NSs. To find the minimum rotational frequency of GW190814’s secondary if it is a pulsar, we focus on the constrained causality surface in the following discussions. Its left boundary is determined by its crossline with the  $R_{1.4} = 12.83$  km (or the very close-by  $\Lambda_{1.4} = 580$ ) surface, while

its right boundary is determined by its crossline with the  $M = 2.14 M_{\odot}$  surface. To be more clear, these crosslines are projected to the  $K_{\text{sym}} - J_{\text{sym}}$  plane in Figure 3. The shadowed range corresponds to the parameters allowed.

We choose 12 parameter sets (black dots) by varying the  $J_{\text{sym}}$  parameter from -200 to 800 MeV along and/or inside the boundaries. The specific values of the  $K_{\text{sym}}$ ,  $J_{\text{sym}}$ , and  $J_0$  parameters and the resulting properties of both non-rotating and uniformly rotating NSs are summarized in Table 1. It is particularly interesting and useful for the following discussions to note that the  $M_{\text{TOV}}$  on the bounded causality surface is between 2.14 and  $2.39 M_{\odot}$ .

**Necessary global properties of GW190814’s secondary component as a fast pulsar:** Using Stergioulas’s RNS code and the 12 EOSs on the causality surface discussed above, we now study the necessary properties for the GW190814’s secondary component to be an NS. For technical and numerical details of the RNS code, we refer the readers to Stergioulas et al. (1995) and its underlying physics to Komatsu et al. (1989); Cook et al. (1994); Stergioulas & Friedman (1995); Nozawa et al. (1998).

For the purposes of this work, we examine the following NS rotational properties:

- The mass-radius relations of fast pulsars with respect to those of non-rotating NSs, including the maximum mass  $M_{\text{TOV}}$  of non-rotating NSs, the pulsar maximum mass  $M_{\text{RNS}}$  at the Kepler frequency  $f_K$  which is the maximum frequency that the gravitational attraction is still sufficient to keep matter bound to the pulsar surface
- The minimum frequency  $f_{2.5}$  (and the ratio  $f_{2.5}/f_K$ ) necessary to rotationally support a pulsar with mass  $2.50 M_{\odot}$  for a given EOS
- The equatorial radius  $R_{\text{RNS}}$  of the pulsar with mass  $M_{\text{RNS}}$ , the equatorial radius  $R_{2.5}$  of the pulsar with mass  $2.50 M_{\odot}$  and frequency  $f_{2.5}$
- The dimensionless spin parameter  $\chi = J/M^2$  where  $J$  is the angular momentum of the pulsar and its minimum value  $\chi_{2.5}$  necessary to support the pulsar with mass  $2.50 M_{\odot}$ .

The mass-radius relations are shown in Figure 3 and the corresponding values of  $M_{\text{TOV}}$ ,  $M_{\text{RNS}}$ ,  $R_{\text{RNS}}$ ,  $R_{2.5}$ ,  $f_{2.5}$ , the ratio  $f_{2.5}/f_K$ , and  $\chi_{2.5}$  are summarized in Table 1. The results for non-rotating NSs are shown with solid lines, while those for pulsars at the Kepler frequency and  $f_{2.5}$  are given with dashed lines and dotted lines, respectively. The reported mass  $2.50 - 2.67 M_{\odot}$  of the secondary in GW190814 is shown as gray bands. Several

interesting observations can be made from these results. We discuss the most important physics points in the following.

- While the  $M_{\text{TOV}}$  of the 12 EOSs are between 2.14 and  $2.39 M_{\odot}$ , pulsars at their respective Kepler frequencies can easily sustain masses heavier than  $2.50 M_{\odot}$ . Of course, the maximum pulsar mass  $M_{\text{RNS}}$  depends sensitively on the EOS and the corresponding  $M_{\text{TOV}}$ . With the stiffest EOS possible, i.e., the EOS1 with  $M_{\text{TOV}} = 2.39 M_{\odot}$ , the  $M_{\text{RNS}} = 2.87 M_{\odot}$ , while with the soft EOSs including EOS3, EOS6, EOS9, and EOS12 on the right boundary of the allowed EOS space shown in Figure 3 that is determined by the causality condition and the  $M = 2.14 M_{\odot}$  surface, the  $M_{\text{RNS}}$  are slightly larger than  $2.50 M_{\odot}$  but less than  $2.67 M_{\odot}$ . Consequently, for these soft EOSs all with the same  $M_{\text{TOV}} = 2.14 M_{\odot}$ , the minimum frequency  $f_{2.5}$  necessary to rotationally support a pulsar with mass  $2.50 M_{\odot}$  should be only slightly smaller than their  $f_K$  values. For this reason, the RNS code does not give the  $f_{2.5}$  pulsar sequences with the EOS3, EOS6, EOS9, and EOS12.
- The mass range on the mass-radius curve with a constant frequency becomes very narrow at higher frequencies (see, e.g., Haensel et al. 2008; Krastev et al. 2008a, for more detailed examples). Indeed, the pulsar sequences at  $f_{2.5}$  shown with the dashed and dotted lines are very flat. As expected, the stiffest EOS needs the lowest value of  $f_{2.5}$ . Thus, as the stiffest EOS allowed, the EOS1 sets the lower limit of  $f_{2.5}$  to  $f_{2.5} > 971$  Hz. Since the frequency of XTE J1739- 285 (Kaaret et al. 2007) at 1122 Hz was not confirmed, the  $f_{2.5}$  is higher than the confirmed highest frequency 716 Hz of PSR J1748-2446ad (Hessels et al. 2006). But it is still much less than the  $f_k$  with  $f_{2.5}/f_K=0.578$ . Obviously, the possibility for GW180814’s secondary as a super-fast pulsar or even the fastest one ever found (Most et al. 2020) cannot be excluded. The critical task is then to get more observational information about the secondary’s spin.
- The minimum value of  $\chi_{2.5}$  corresponding to the minimum  $f_{2.5}$  is 0.375 with the stiffest EOS, namely the EOS1. Since the fixed frequency pulsar sequences cannot be calculated with the RNS code when the  $f_{2.5}$  approaches the Kepler frequency as we discussed above, the upper boundary of  $\chi_{2.5}$  is not determined here. However, it should be smaller than the maximum spin parameter  $\chi_{\text{max}}$ , which is around 0.6 – 0.7 and model-

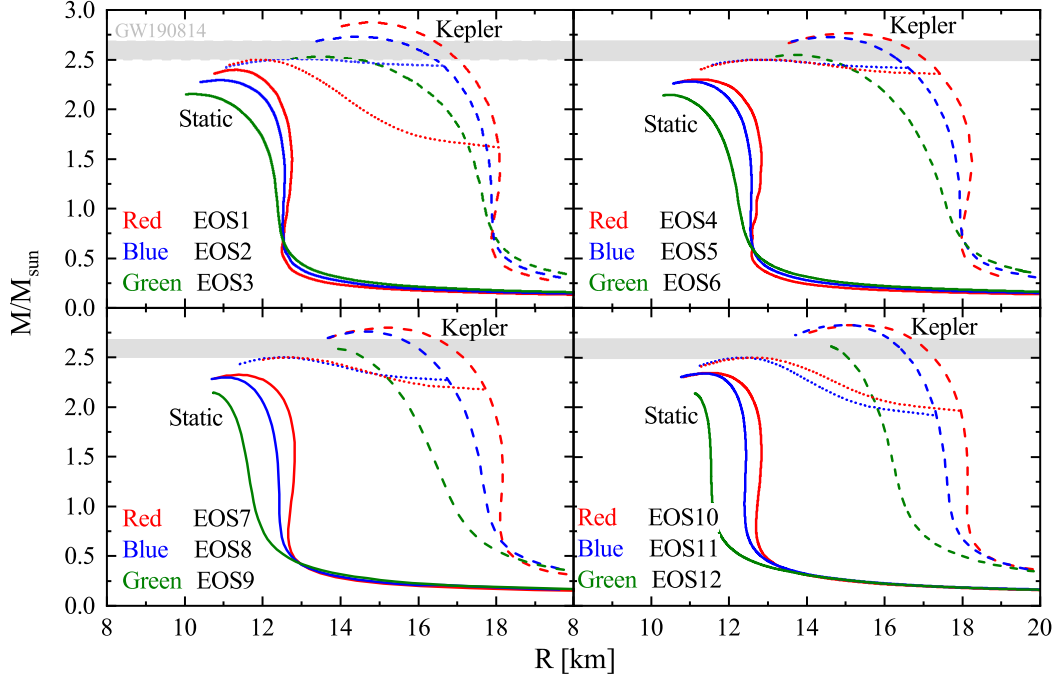


**Figure 4.** The M-R relations for static (solid lines) and rapidly rotating neutron stars for the parameter sets shown in Figure 3. The neutron stars rotating at Kepler frequency and minimum frequency that can support a neutron star with  $2.50 M_{\odot}$  are shown as dashed lines and dotted lines, respectively. The reported mass  $2.50 - 2.67 M_{\odot}$  of GW190814's secondary component is shown as gray bands.

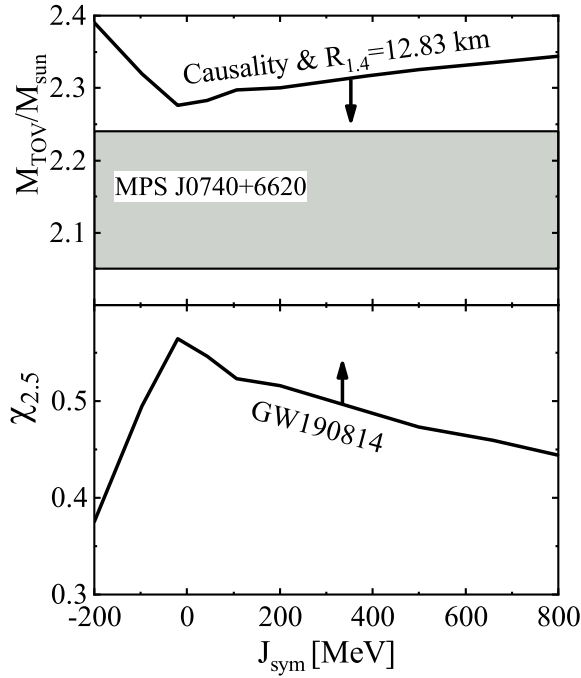


**Figure 5.** The maximum mass  $M_{\text{TOV}}$  of non-rotating NSs (upper window) and the minimum spin parameter  $\chi_{2.5}$  of pulsars with the frequency  $f_{2.5}$  (lower window) as functions of the high-density symmetry energy parameter  $J_{\text{sym}}$ . The currently observed NS maximum mass  $M = 2.14^{+0.10}_{-0.09} M_{\odot}$  (68% confidence level) of MSR J0740+6620 is shown in the upper panel. The arrows indicate the conditions for GW190814's secondary to be a super-fast pulsar.

independent (Friedman & Ipser 1992; Lo & Lin 2011). As shown in Figure 2, the causality surface goes downwards towards its crossline with the  $2.14 M_{\odot}$  surface, namely, the EOS becomes softer with the decreasing  $K_{\text{sym}}$  when the  $J_{\text{sym}}$  is fixed. As a result, as shown in Table 1, the  $M_{\text{TOV}}$ ,  $f_{2.5}$ , and  $\chi_{2.5}$  all decrease correspondingly. Thus, the left boundary of the projected EOS space shown in Figure 3 provides the lower boundary of  $\chi_{2.5}$  and the upper boundary of  $M_{\text{TOV}}$ . As shown in Figure 2, this is the boundary set by the crossline between the causality surface and the surface with a constant radius of  $R_{1.4} < 12.83$  km.

- The maximum mass  $M_{\text{TOV}}$  of non-rotating NSs (upper window) and the corresponding minimum spin parameter  $\chi_{2.5}$  of pulsars with the frequency  $f_{2.5}$  (lower window) are shown in Figure 5 as functions of the parameter  $J_{\text{sym}}$ . As we discussed earlier, the latter controls the behavior of nuclear symmetry energy at densities above  $2\rho_0$ . It is currently considered as the most uncertain parameter of the EOS of super-dense neutron-rich nucleonic matter (Li 2017). For a comparison, the mass  $M = 2.14^{+0.10}_{-0.09} M_{\odot}$  (68% confidence level) of MSR J0740+6620 is also shown in the upper panel. The arrows indicate the conditions for GW190814's secondary component to be a super-fast pulsar with its minimum spin parameter  $\chi_{2.5}$ .

Combining the information from this plot and the constrained EOS parameter space shown in Figure 2, clearly all the EOSs in the whole space between the causality surface and the  $M = 2.14 M_{\odot}$  surface can support pulsars as heavy as  $2.50 M_{\odot}$  if they rotate with varying minimum frequencies higher than 971 Hz depending on the symmetry energy of super-dense neutron-rich nuclear matter. This further illustrates the importance of better constraining the latter with terrestrial experiments and/or astrophysical observations.

- The stiffest EOS, EOS1 ( $K_{\text{sym}} = 33$  MeV,  $J_{\text{sym}} = -200$  MeV and  $J_0 = 112.5$  MeV) requires the least spin parameter  $\chi_{2.5} = 0.375$ . The corresponding  $M_{\text{TOV}}=2.39 M_{\odot}$  is a little higher than the  $M_{\text{TOV}}=2.3 M_{\odot}$  adopted by [Most et al. \(2020\)](#) from analyzing GW170817. Using the latter and assuming the radius of GW190814’s secondary is 13 km, they extracted a range of  $0.49 < \chi < 0.68$  and  $f > 1140$  Hz for the spin parameter based on the universal relations of masses and spin parameters ([Breu & Rezzolla 2016](#)). Our results are qualitatively consistent and the quantitative difference can be well understood from the differences in the  $M_{\text{TOV}}$  and the pulsar radius used.
- There are some longstanding and interesting issues regarding the stability of fast pulsars (see, e.g., [Hessels et al. 2006](#); [Haensel et al. 2008](#)), such as the r-mode instability in the cores of fast pulsars (see, e.g., [Lindblom et al. 1998](#); [Owen et al. 1998](#); [Andersson et al. 2001](#); [Levin & Ushomirsky 2001](#)) that may happen at frequencies much lower than the Kepler frequency. The r-mode instability window depends strongly on the core temperature and its transport properties as well as the coupling with and structure of the crust. Its calculation is still very model dependent and relies on many poorly known properties of NS matter. For instance, it has been shown by [Wen et al. \(2012\)](#) and [Vidaña \(2012\)](#) that both the Kepler frequency  $f_K$  and the boundaries of the r-mode instability window in the frequency-temperature plane have significant dependencies on nuclear symmetry energy. The separation between the  $f_K$  and the critical frequency  $f_r$  above which the r-mode instability occurs is strongly temperature dependent. How the minimum frequency  $f_{2.5}$  for the GW190814’s secondary component to be a super-fast pulsar compares with the critical r-mode instability frequency  $f_r$  is an interesting question for future studies.

**Summary and Conclusion:** Using Stergioulas’s RNS code for investigating fast pulsars with EOSs

on the causality surface and allowed by all known constraints from both nuclear physics and astrophysics, we found that the GW190814’s secondary component can be a super-fast pulsar as long as it rotates faster than 971 Hz about 42% below its Kepler frequency. There is a large high-density EOS parameter space below the causality surface permitting pulsars heavier than  $2.50 M_{\odot}$  if they can rotate even faster with varying critical frequencies depending strongly on the high-density behavior of nuclear symmetry energy. To rule out completely the possibility for the GW190814’s secondary component as a super-fast pulsar, it is critical to observationally constrain its spin properties. To better understand the properties of super-fast pulsars it is important to further constrain the high-density behavior of nuclear symmetry energy with both astrophysical observations and terrestrial nuclear experiments.

**Acknowledgement:** We would like to thank Dr. Ronaldo Vieira Lobato for useful communications. This work is supported in part by the U.S. Department of Energy, Office of Science, under Award Number DE-SC0013702, the CUSTIPEN (China-U.S. Theory Institute for Physics with Exotic Nuclei) under the US Department of Energy Grant No. DE-SC0009971, the China Postdoctoral Science Foundation under Grant No. 2019M652358, and the Fundamental Research Funds of Shandong University under Grant No. 2019ZRJC001.

## REFERENCES

Abbott, B. P., Abbott, R., Abbott, T. D., et al. 2020, ApJL, 896, L44

Abbott, B. P., Abbott, R., Abbott, T. D., et al. 2018, PhRvL, 121, 161101

Andersson, N., & Kokkotas, K. D. 2001, IJMPD, 10, 381

Baym, G., Pethick, C. J., & Sutherland, P. 1971, ApJ, 170, 299

Bombaci, I., & Lombardo, U. 1991, PhRvC, 44, 1892

Breu, C., & Rezzolla, L. 2016, MNRAS, 459, 646

Brown, B. A., & Schwenk, A. 2014, PhRvC, 89, 011307, Erratum: [2015, PhRvC, 91, 049902].

Cook, G. B., Shapiro, S. L., & Teukolsky, S. A. 1994, ApJ, 422, 227

Cromartie, H. T., Fonseca, E., Ransom, S. M., et al. 2019, NatAs, 4, 72

Fishbach, M., Essick, R., & Holz, D. E. 2020, arXiv:2006.13178

Friedman, J. L., & Ipser, J. R. 1992, Philos. Trans. R. Soc. London, Ser. A, 340, 391

Garg, U., & Colò, G. 2018, Prog. Part. Nucl. Phys., 101, 55

Haensel, P., Zdunik, J. L., & Bejger, M. 2008, New Astronomy Review, 51, 785

Haensel, P., Zdunik, J. L., Bejger, M., & Lattimer, J. K. 2009, A&A, 502, 605

Hessels, J. W. T., Ransom, S. M., Stairs, I. H., Freire, P. C. C., Kaspi, V. M., & Camilo, F. 2006, Sci, 311, 1901

Kaaret, P., Prieskorn, Z., in't Zand, J. J. M., Brandt, S., Lund, N., Mereghetti, S., Götz, D., Kuulkers, E., & Tomsick, J. A. 2007, ApJ, 657, L97

Komatsu, H., Eriguchi, Y., & Hachisu, I. 1989, MNRAS, 237, 355

Krastev, P. G., Li, B. A., & Worley, A. 2008, ApJ, 676, 1170

Krastev, P. G., Li, B. A., & Worley, A. 2008, Phys. Lett. B, 668, 1

Lasota, J. P., Haensel, P., & Abramowicz, M. A. 1996, ApJ, 456, 300

Lattimer, J. M., & Prakash, M. 2000, Phys. Rep., 333, 121

Lattimer, J. M., & Prakash, M. 2004, Sci, 304, 536

Lattimer, J. M., & Steiner, A. W. 2014, Eur. Phys. J. A, 50, 40

Lehmann, B. V., Profumo, S., & Yant, J. 2020, arXiv:2007.00021

Levin, Y., & Ushomirsky, G., 2001, Mon. Not. R. Astron. Soc., 324, 917

Li, B. A., & Steiner, A. W. 2006, Phys. Lett. B, 642, 436

Li, B. A., Chen, L. W., & Ko, C. M. 2008, Phys. Rep., 464, 113

Li, B. A., & Han, X. 2013, Phys. Lett. B, 727, 276

Li, B. A., Ramos, Á., Verde G., & Vidaña, I. (Eds.) 2014, *Topical Issue on Nuclear Symmetry Energy*, Eur. Phys. J. A, 50, 9

Li, B. A. 2017, Nuclear Physics News, 27, 7

Li, B. A., Krastev, P. G., Wen, D. H., & Zhang, N. B. 2019, Euro. Phys. J. A, 55, 117

Lindblom, L., Owen, B. J., & Morsink, S.M., PhRvL80, 4843

Lo, K. W., & Lin, L. M. 2011, ApJ, 728, 12

Miller, M. C., Lamb, F. K., Dittmann, A. J., et al. 2019, ApJL, 887, L24

Most, E. R., Jens Papenfort, L., Weih, L. R., & Rezzolla, L. 2020, arXiv:2006.14601

Negele, J. W., & Vautherin, D. 1973, NuPhA, 207, 298

Nozawa T., Stergioulas N., Gourgoulhon E., & Eriguchi Y. 1998, A&A, 132, 431

Oertel, M., Hempel, M., Klähn, T., & Typel, S. 2017, Rev. Mod. Phys., 89, 015007

Oppenheimer, J., & Volkoff, G. 1939, Phys. Rev., 55, 374

Owen, B.J. et al., 1998, PhRvD, 58, 084020

Piekarewicz, J. 2010, JPhG, 37, 064038

Riley, T. E., Watts, A. L., Bogdanov, S., et al. 2019, ApJL, 887, L21

Shlomo, S., Kolomietz, V. M., & Colò G. 2006, Eur. Phys. J. A, 30, 23

Stergioulas, N. et al., 1995, RNS code, <http://www.gravity.phys.uwm.edu/rns/>

Stergioulas N., & Friedman J. L., 1995, ApJ, 444, 306

Tan, H., Noronha-Hostler, J., & Yunes, N., 2020, arXiv:2006.16296

Tews, I., Lattimer, J. M., Ohnishi, A., & Kolomeitsev, E. E. 2017, ApJ, 848, 105

Tolman, R. C. 1934, Proc. Natl. Acad. Sci. U.S.A., 20, 3

Vidaña, I. 2012, PhRvC, 85, 045808

Worley, A., Krastev, P. G., & Li, B. A. 2008, ApJ, 685, 390

Wei, J. B., Chen, H., Burgio, G. F., & Schulze, H. J. 2017, PhRvD, 96, 043008.

Wen, D. H., Newton, W. G., & Li, B. A. 2012, PhRvC, 85, 025801

Xie, W. J., & Li, B. A. 2019, ApJ, 883, 174

Xie, W. J., & Li, B. A. 2020, arXiv:2005.07216, APJ in press.

Zhang, N. B., Cai, B. J., Li, B. A., Newton, W. G., & Xu, J. 2017, Nucl. Sci. Tech., 28, 181

Zhang, N. B., Li, B. A., & Xu, J. 2018, ApJ, 859, 90

Zhang, N. B., & Li, B. A. 2019, Eur. Phys. J. A, 55, 39

Zhang, N. B., & Li, B. A. 2019, JPhG, 46, 014002

Zhang, N. B., & Li, B. A. 2019, ApJ, 879, 99

Zhang, N. B., & Li, B. A. 2020, ApJ, 883, 61